3922 J. Phys. Chem. A 2009, 113, 3922–3931

Experimental and Theoretical Study of Rotationally Inelastic Collisions of CN($A^2\Pi$) with N_2[†]

Ani Khachatrian,[‡] Paul J. Dagdigian,*[,‡] Doran I. G. Bennett,[§,||] François Lique,[§,⊥] Jacek Kłos,[§] and Millard H. Alexander*[,§]

Department of Chemistry, The Johns Hopkins University, Baltimore, Maryland 21218-2685, and Department of Chemistry and Biochemistry and Institute for Physical Science and Technology, University of Maryland, College Park, Maryland 20742-2021

Received: November 18, 2008; Revised Manuscript Received: January 6, 2009

Optical−optical double resonance was employed to study rotational energy transfer in collisions of selected rotational/fine-structure levels of CN($A^2\Pi$, $v = 3$) with N_2. The CN radical was generated by 193 nm photolysis of BrCN in a slow flow of N_2 at total pressures of 0.2−1.4 Torr. Specific fine-structure Λ-doublet levels of CN($A^2\Pi$, $v = 3$) were prepared by pulsed dye laser excitation on isolated lines in the CN $A-X$ (3,0) band, while the initially excited and collisionally populated levels were observed after a short delay by laser-induced fluorescence in the $B-A$ (3,3) band. Total removal rate constants for specified rotational/fine-structure levels involving total angular momentum J from 4.5 to 12.5 were determined. These rate constants decrease with increasing J, with no obvious dependence on the fine-structure/Λ-doublet label. State-to-state relative rate constants were determined for several initial levels and show a strikingly strong collisional propensity to conserve the fine-structure/Λ-doublet label. Comparison is made with the results of quantum scattering calculations based on potential energy surfaces averaged over the orientation of the N_2 molecule. Reasonable agreement is found with experimentally determined total removal rate constants. However, the computed state-to-state rate constants show a stronger propensity for fine-structure and Λ-doublet changing transitions. These differences between experiment and theory could be due to the neglect of the N_2 orientation and the correlation of the CN and N_2 angular motions.

1. Introduction

Rotationally inelastic collisions of diatomic molecules in Π electronic states have been of considerable interest[1] because, in contrast to collisions of closed-shell diatomics, the collision of a Π-state molecule with an atom or another molecule can alter both the rotational angular momentum and the fine-structure/Λ-doublet label. Collisions of molecules in Π states are the simplest molecular collisional rate process which necessarily involves more than one Born−Oppenheimer potential energy surface (PES). The orbital degeneracy of the Π state is removed by approach of a collision partner, and the interaction can be described by two PESs, of A' and A'' symmetry for a structureless target.

In previous investigations,[2−10] Dagdigian, Alexander, and co-workers have carried out extensive experimental and theoretical state-to-state studies of rotational and electronic energy transfer of CN($A^2\Pi$) with the rare gases helium and argon. The experiments involved the optical−optical double resonance (OODR) technique to populate specific initial rotational/fine-structure levels in the $A^2\Pi$ state and to detect the collisionally populated final levels. Theoretical study of CN−rare gas collisions is facilitated by the fact that the PESs depend on only two nuclear coordinates, in contrast to collisions with molecular partners, and it has been possible to make detailed comparisons of experimental rate constants with computed values obtained from quantum scattering calculations. In recent work, Alagappan et al.[11] have investigated state- and velocity-changing collisions of CN($A^2\Pi$) by Doppler-resolved frequency-modulated spectroscopy in collisions with He, Ar, N_2, and O_2. With this technique, it has been possible to obtain state-to-state differential cross sections.[12]

Other groups have carried out similar state-to-state investigations of rotational energy transfer in other electronic states of CN. Fei et al.[13,14] employed stimulated emission pumping to prepare the initial state in their studies of rotational energy transfer in the CN($X^2\Sigma^+$, $v = 2$) manifold in collisions with He and Ar. More recently, Smith and co-workers[15,16] have employed IR−optical double resonance to determine CN($X^2\Sigma^+$, $v = 2$)−N_2, C_2H_2 state-resolved rate constants. Sadowski and co-workers[17,18] have employed resolved fluorescence spectroscopy to study rotational energy transfer in the CN($B^2\Sigma^+$) state. In studies of both the $X^2\Sigma^+$ and $B^2\Sigma^+$ states, the spin splittings were not resolved.

In the present paper, we extend our study of state-to-state collisions of CN($A^2\Pi$) to a molecular collision partner, namely, N_2. We report here total removal rate constants for selected rotational/fine-structure levels in the CN($A^2\Pi$, $v = 3$) vibronic manifold. It is of interest to probe the dependence of these rate constants upon the total angular momentum J and fine-structure/Λ-doublet label. In addition, we compare these measured rate constants with our previously reported values for Ar as the collision partner, as well as those determined for collisions of CN($X^2\Sigma^+$, $v = 2$) with N_2, determined by Olkhov and Smith.[16]

[†] Part of the "George C. Schatz Festschrift".

* Corresponding authors, pjdagdigian@jhu.edu and mha@umd.edu.

[‡] The Johns Hopkins University.

[§] University of Maryland.

[||] Present address: Department of Chemistry, University of California, Berkeley, CA 94720-1460.

[⊥] Present address: LOMC, Université du Havre, 25 Rue Philippe Lebon, BP 540, 76 058 Le Havre cedex, France.

10.1021/jp810148w CCC: $40.75

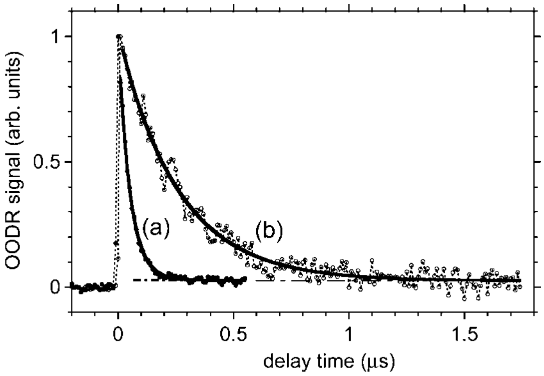

Figure 1. OODR signals (open circles, connected with dotted lines) for the detection of CN ($A^2\Pi$, $v = 3$, $J = 7.5$ F_1f) radicals as a function of time delay between pump and probe laser pulses in a mixture of 0.01 Torr BrCN and (a) 1.1 and (b) 0.15 Torr N_2, respectively. The pump laser was tuned to the $A-X$ (3,0) $Q_1(7)$ line, while the probe laser was tuned to the $B-A$ (3,3) $Q_1(7)$ line. The heavy solid lines are nonlinear least-squares fits of the decay profiles to exponential functions (see text). The fitted baseline at long delay times is indicated by a dot-dashed line.

Chemical reaction is not possible in collisions of CN($A^2\Pi$) with N_2. Collisional removal of CN($A^2\Pi$) levels can thus occur only by rotational, vibrational, or electronic transitions. Room-temperature rate constants for the electronic quenching of CN($A^2\Pi$) have been reported in several studies.[19-21] Halpern et al.[21] report a value of $(2.4 \pm 0.2) \times 10^{-11}$ cm^3 molecule^{-1} s^{-1} for the room-temperature quenching rate constant for CN($A^2\Pi$, $v = 3$) in collisions with N_2. This rate constant pertains to the collisional removal of a room-temperature rotational state distribution. As we show below, the total removal rate constants for specified CN($A^2\Pi$, $v = 3$) rotational/fine-structure levels are much larger, reflecting that the latter rate constants are a measure predominantly of the much faster rate of rotational energy transfer.

State-to-state rate constants reflect more directly the topology of the PESs than do total removal rate constants. We also present state-to-state relative rate constants for collision-induced rotational/fine-structure transitions out of several initial levels. Our experimental data show a strikingly strong collisional propensity to conserve the fine-structure/Λ-doublet label, in contrast to collisions with argon.[9]

Finally, we compare the total removal rates constants and selected state-to-state relative rate constants with the results of quantum scattering calculations based on a new ab initio potential energy surface, averaged over the orientation of the N_2 molecule.

2. Experimental Section

Optical−optical double resonance (OODR) was employed for the study of rotational energy transfer within the CN($A^2\Pi$) state in collisions with N_2. The apparatus employed was similar to that used in our previous studies of CN($A^2\Pi$) energy transfer.[7-10] CN radicals were generated by pulsed 193 nm photolysis of BrCN (Aldrich, 99.995%), which was bled into the central part of the vacuum chamber, while nitrogen (99.998%) was introduced through the ends of the chamber sidearms. Typical partial pressures were 0.01 Torr BrCN and 0.2−1.4 Torr N_2. The absolute pressure was determined with a capacitance manometer (MKS).

The central 15 mm diameter portion (10 mJ/pulse entering the chamber) of a 193 nm excimer laser (Lambda Physik COMPex 102) beam entered the chamber through one of the sidearms. The tunable pump and probe laser beams (both with ~0.2 cm^{-1} spectral bandwidths) were overlapped with a dichroic mirror and entered the chamber from the opposite sidearm and counterpropagated with the excimer laser beam. The pump laser was tuned to an isolated line in the CN $A^2\Pi-X^2\Sigma^+$ (3,0) band to excite molecules to a given rotational/fine-structure level in the $v_A = 3$ vibronic manifold, while the probe laser was tuned through the $B^2\Sigma^+-A^2\Pi$ (3,3) band to detect the initially excited and collisionally populated levels. The pump beam (7 mJ in 1.5 mm diameter entering the apparatus) was the output of a dye laser (Lambda Physik FL3002) pumped with the 532 nm output of a Nd:YAG laser (Continuum NY-81C), while the probe beam (0.5 mJ in 1.5 mm diameter entering the apparatus) was the output of a homemade dye laser pumped with the 355 nm output of a Nd:YAG laser (Continuum Precision 8000).

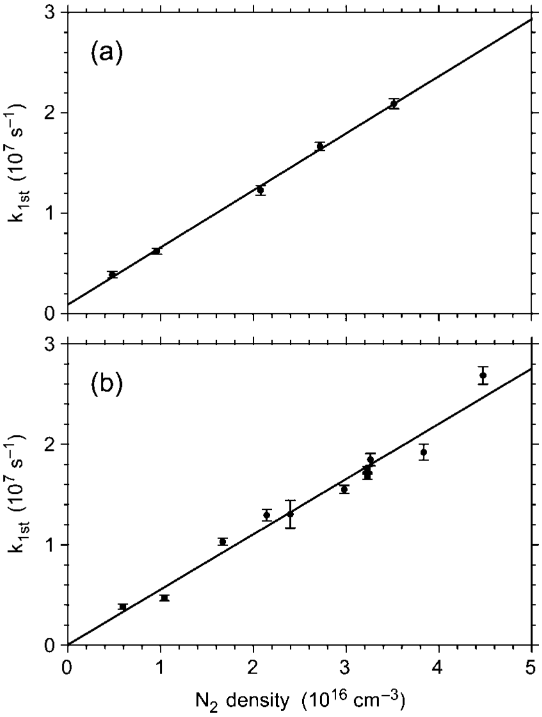

Figure 2. Plots of the determined pseudo-first-order decay rates for the removal of CN($A^2\Pi$, $v = 3$) in the (a) $J = 5.5$ F_1e and (b) $J = 11.5$ F_2f rotational/fine-structure levels as a function of the concentration of N_2. The partial pressure of BrCN was 0.01 Torr. The straight lines are weighted linear least-squares fits to the data.

The delays between the three lasers were controlled with a digital pulse generator (Berkeley Nucleonics BNC 555). The delay between the photolysis and pump lasers was 25 and 200 μs for the measurement of total removal rate constants and state-to-state rate constants, respectively. At these delays, scans of the $A-X$ (3,0) band can be characterized with a room-temperature rotational state distribution; hence, the CN translational energy distribution is also expected to follow a room-temperature Maxwellian distribution. Variable pump−probe delays, which were set within the data acquisition program, were employed for the determination of state-selected total removal rate constants.

Olkhov and Smith[16] have considered in detail the thermalization of CN in the rotational energy transfer studies of CN($X^2\Sigma^+$, $v = 2$) by the use of two different photolytic precursors, namely, the 266 nm photolysis of ICN and the 570 nm photolysis of NCNO. The former production method generates translationally hot CN, while the latter forms radicals with a near room-temperature translational energy distribution.

TABLE 1: Total removal rate constants (in units of 10^{-10} cm^3 molecule^{-1} s^{-1}) at 293 K for specified rotational/fine-structure levels of CN($A^2\Pi$, v=3) in collisions with N_2[a]

	F_1 fine-structure levels			F_2 fine-structure levels		
J	energy[b]	F_1e (A')[c]	F_1f (A'')	energy[b]	F_2f (A')	F_2e (A'')
4.5				91.8		6.13 ± 0.76 4.63
5.5	51.4	5.50 ± 0.36 4.98	5.73 ± 0.46 4.84	110.5		5.51 ± 0.91 4.58
7.5	96.5		5.23 ± 0.20 4.71			
9.5				219.2	4.81 ± 0.31 4.31	
10.5	188.3		5.35 ± 0.36 4.48			
11.5				293.8	4.82 ±0.38 4.13	
12.5	265.8		4.95 ± 0.77 4.30			

[a] Quoted uncertainties are 2σ. The upper and lower entries correspond, respectively, to the expermentally measured and theoretically simulated (eq 5) rate constants. [b] Energy (in cm^{-1}) relative to the lowest level (J = 1.5 F_1e/f) in the CN($A^2\Pi$, v = 3) manifold. For these levels, the Λ-doubling is <0.1 cm^{-1}. [c] The symmetry of the Λ-doublet levels in the high-J limit is indicated.

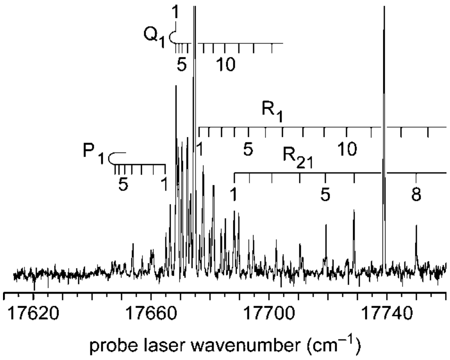

Figure 3. OODR laser-induced fluorescence spectrum of the $B^2\Sigma^+-A^2\Pi$ (3,3) band. The J = 7.5 F_1f initial level was prepared by pump laser excitation of the $Q_1(7)$ line of the $A^2\Pi-X^2\Sigma^+$ (3,0) band; the pump−probe delay was 10 ns. The partial pressures of BrCN and N_2 were 0.01 and 0.3 Torr, respectively, and the photolysis−pump delay was 200 μs. The rotational lines are identified with the rotational angular momentum N of the CN($A^2\Pi$, v = 3) levels.

They found that the total removal rate constants with the NCNO precursor are essentially independent of the photolysis−pump delay, while rate constants measured with the ICN precursor are larger for short delays and approach values with NCNO precursor for pressure-delay products of ~1 Torr μs. Similar to the situation with ICN, the photolysis of BrCN yields translationally hot radicals. With our range of pressures (0.2−1.4 Torr) and a ≥25 μs photolysis−probe delay, the CN radicals in our experiment should be well equilibrated translationally.

Fluorescence was observed with two separate detectors, which observed the $A-X$ fluorescence signal induced by the pump laser and the $B-X$ OODR signal excited by the probe laser. The transient signals from the photomultipliers were directed to gated integrators (Stanford Research Systems SR250), and the outputs were collected under computer control and stored on magnetic media for later analysis. For some wavelength regions, particularly to the blue of the $B-A$ (3,3) band origin, the probe laser alone excited $B-X$ fluorescence due to the presence of vibrationally excited CN($X^2\Sigma^+$) from the photolysis and partial collisional relaxation. For the range of rotational levels studied, the probe-only fluorescence signals did not occur in the same spectral range as the OODR signals.

The intensity of the pump laser was sufficiently high to essentially saturate the $A-X$ transition. Hence, the initially excited rotational level should have an isotropic M_J distribution. In contrast to earlier studies,[7−10] in which low laser power was employed for excitation of the $B-A$ transition, higher probe laser powers were used in the present set of experiments. This causes no complications in the determination of total removal rate constants since only one rotational/fine-structure level in the A state is detected. Line strength factors appropriate to saturation conditions[22,23] were employed to convert intensities (peak areas) in the OODR spectra to populations.

3. Experimental Results

A. Total Removal Rate Constants. Total removal rate constants from specified rotational/fine-structure levels in the CN($A^2\Pi$, v = 3) manifold in collisions with N_2 were determined by laser-induced fluorescence detection in the $B-A$ (3,3) band of the initially excited levels as a function of the pump−probe delay. Plots of the typical decay of the OODR signal for detection of the initially excited level versus the pump−probe delay are displayed in Figure 1 for one initial level at two different N_2 concentrations. The OODR signal is found to decay exponentially after the probe laser pulse, at a rate dependent upon the N_2 concentration. It can be seen that the signal at long delay times is slightly above the baseline (represented by the signal at negative pump−probe delay times). This nonzero signal at long delay times is a result of the collisional thermalization of the initially excited population to room-temperature Boltzmann distributions of the rotational/fine-structure populations in the CN($A^2\Pi$, v = 3) manifold. This thermalization leaves some population in the initially excited level. This behavior was also observed by Smith and co-workers[15,16,24] in their CN($X^2\Sigma^+$, v = 2) rotational energy transfer experiments. At much longer times, the population in the CN($A^2\Pi$, v = 3) manifold decays through collision-induced electronic and vibrational transitions.

As the concentration of CN($A^2\Pi$, v = 3) was much lower than that of the N_2 collision partner (including the low concentration of the BrCN photolytic precursor), data such as those displayed in Figure 1 were analyzed to determine pseudo-first-order decay rates of the initially excited CN($A^2\Pi$, v = 3) rotational fine-structure levels. The OODR signal over the time range starting 10 ns after the probe laser beam to the end of the

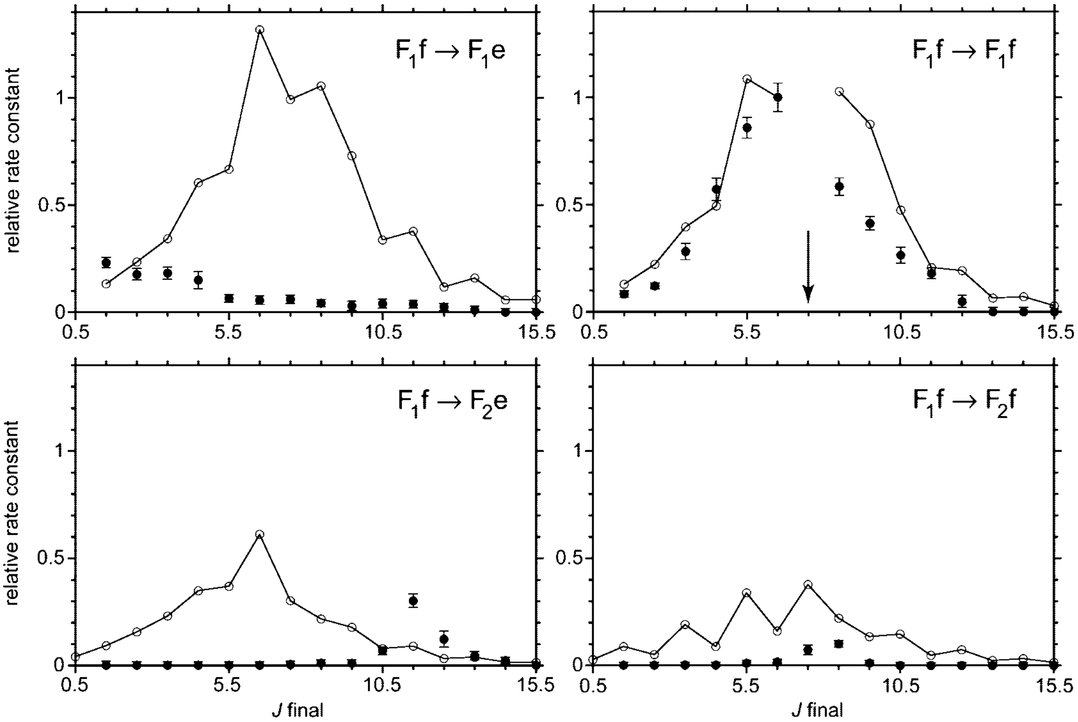

Figure 4. Relative room-temperature rate constants for transfer out of the $J = 7.5$ F_1f level of CN($A^2\Pi$, $v = 3$) in collisions with N_2. The four panels correspond to each of the four possible spin−orbit/Λ-doublet combinations of the final level. The solid circles with error bars are the experimental measurements, and the open circles connected with solid lines are the results of the scattering calculations. All rate constants have been normalized to the $J = 7.5$ $F_1f \rightarrow J = 6.5$ F_1f transition. The initial level is denoted with an arrow.

time delay scan was fitted to the determine pseudo-first-order decay rates k_{first}. The decay profiles were fitted to the functional form

$$I(t) = A \exp(-kt) + B \tag{1}$$

by a nonlinear least-squares procedure. The thick solid lines in Figure 1 show the results of such fits. The baseline B in each plot is indicated by a dot-dashed line.

Since the baseline B is not zero because of the rotational equilibration, the fitted decay rates k are not strictly equal to the pseudo-first-order total removal rate constants. Following Olkhov and Smith,[16] we included an approximate correction for back transfer into the initial level. Approximating the equilibration in a two-state kinetic model (initial level and all other levels in the vibronic manifold), k_{first} was computed from the fitted values of k, A, and B as follows

$$k_{\text{first}} = k\frac{A}{A+B} \tag{2}$$

This correction for back transfer was of the order of 3−10% for the levels investigated.

For each initial level investigated, OODR signal decays were recorded over a range of N_2 concentrations, and each decay profile was analyzed to determine a first-order decay rate k_{first}. The determined decay rates for two different initial levels as a function of the N_2 concentration are plotted in Figure 2. These decay rates versus concentration were fitted to a straight line, as illustrated in Figure 2, and the bimolecular total removal rate constants were determined from the slopes of the fitted lines. It can be seen in Figure 2 that the fitted lines do not go through the origin. The decay rate extrapolated to zero N_2 concentration can be ascribed to relaxation by the low concentration of the BrCN photolytic precursor and physical loss of radicals out of the detection zone.

Levels significantly populated in a room-temperature state distribution in each of the four fine-structure/Λ-doublet manifolds were investigated. It should be noted that the lower rotational levels within a given CN($A^2\Pi$) vibrational manifold follow Hund's case (a) fairly closely. In this limit, the electron spin is strongly coupled to the internuclear axis and can couple to the electronic orbital angular momentum projection Λ, leading to two fine-structure manifolds with molecule-fixed projection $\Omega = \Lambda + \Sigma = 1/2$ and $3/2$ (labeled F_2 and F_1, respectively, since the spin−orbit constant A is negative[25] for CN($A^2\Pi$)). Because of the orbital degeneracy of a Π electronic state, the levels appear as nearly degenerate pairs of opposite total parity, i.e., the Λ-doublets, which are labeled[26] *e* and *f* for total parity $+(-1)^{J-1/2}$ and $-(-1)^{J-1/2}$, respectively.

Total removal rate constants for collisions of a number of CN($A^2\Pi$, $v = 3$) rotational fine-structure levels were determined and are listed in Table 1. For convenience, the rotational energies of all levels investigated are also listed in Table 1. (For a rotational energy diagram of the CN($A^2\Pi$, $v = 3$) manifold, see Figure 5 of ref 9.) Spectral overlaps at our dye laser resolution in the $A-X$ (3,0) band limited the levels which could be selectively excited. The levels for which rate constants were reported in Table 1 could all be excited cleanly on resolved $A-X$ lines. We observe a modest decrease, but within the experimental uncertainties, in the total removal rate constant with increasing total angular momentum J. No obvious dependence upon the fine-structure/Λ-doublet label is discernible. These rate constants are compared in section 6 with total removal rate constants of CN($A^2\Pi$, $v = 3$) levels in collisions with Ar, previously reported by our group[9] and of CN($X^2\Sigma^+$, $v = 3$) levels in collisions with N_2, reported by Olkhov and Smith.[16]

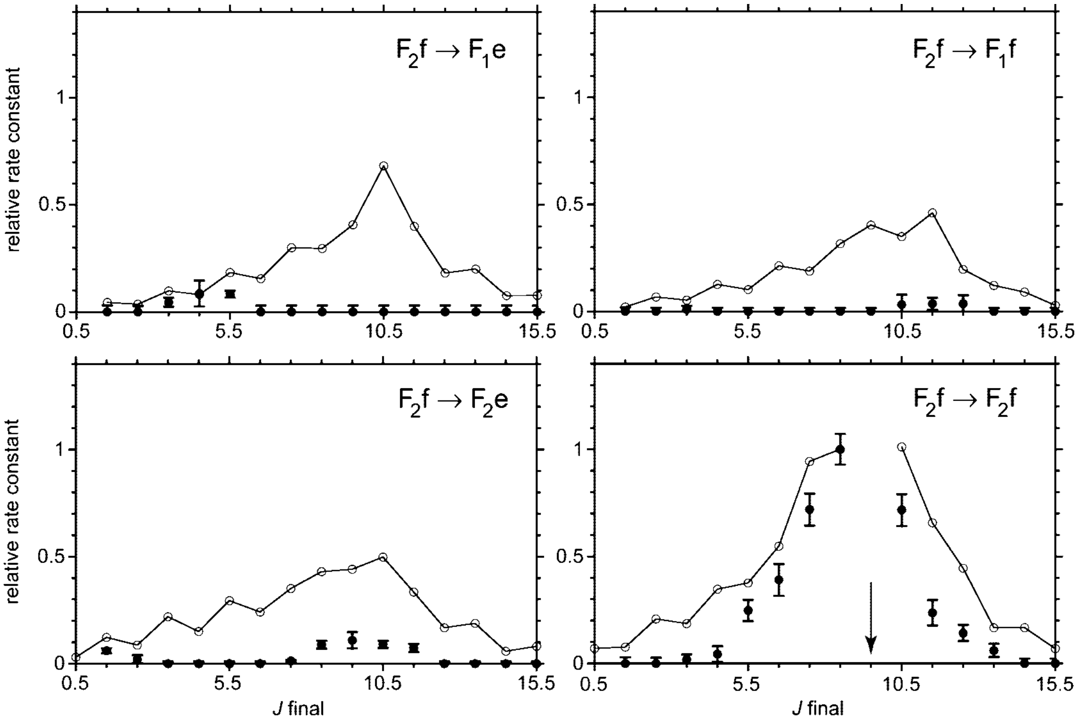

Figure 5. Relative room-temperature rate constants for transfer out of the $J = 9.5$ F_2f level of CN($A^2\Pi$, $v = 3$) in collisions with N_2. The four panels correspond to each of the four possible spin−orbit/Λ-doublet combinations of the final level. The solid circles with error bars are the experimental measurements, and the open circles connected with solid lines are the results of the scattering calculations. All rate constants have been normalized to the $J = 9.5$ $F_2f \rightarrow J = 8.5$ F_2f transition. The initial level is denoted with an arrow.

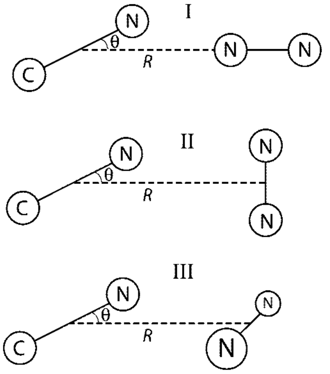

Figure 6. Schematic illustration of the three geometries at which ab initio calculations were performed. The arrangement of the N_2 molecule was held fixed, in each case, while the angle θ and center-of-mass separation R were varied. The angle $\theta = 0$ corresponds to the N-end of the CN molecule pointing toward the N_2 molecule. Geometries I and II are coplanar, while in geometry III the N_2 molecule is perpendicular to the plane of rotation of the CN molecule.

B. Relative State-to-State Rate Constants. It is well-known that rate constants for transitions between specified pairs of rotational/fine-structure levels are much more sensitive to the form of the potential energy surfaces than are the total removal rate constants, as illustrated by our previous work on CN($A^2\Pi$)−Ar, He collisions.[7−10] Figure 3 displays an OODR spectrum for the $J = 7.5$ F_1f initial level at a short pump−probe delay (10 ns). The two intense lines in the spectrum involve detection of the initially pumped level. The only rotational branches in the spectrum with large intensity are the Q_1 and R_{21} branches, which probe levels in the same fine-structure/Λ-doublet manifold as the initial level. Lines in the P_1 and R_1 branches also appear with weaker intensities. With the exception of several lines in the Q_2 branch near the $Q_1(7)$ line, lines probing levels in the F_2 fine-structure manifold were very weak or not observed (see Figure 3). Thus, the line intensities in the OODR spectrum strongly suggest a substantial propensity to conserve the fine-structure/Λ-doublet label.

Spectra such as that shown in Figure 3 were employed to determine relative state-to-state rate constants. We plot in Figure 4 the relative state-to-state rate constants obtained for collisional transfer out of the $J = 7.5$ F_1f initial level. These data confirm the qualitative conclusion drawn from examination of the OODR spectrum displayed in Figure 3. Figure 5 presents relative state-to-state rate constants for transitions out of a level in the F_2 fine-structure manifold, namely, the $J = 9.5$ F_2f level. We see that the propensity to conserve the fine-structure/Λ-doublet label is even stronger for this initial level. Preliminary data were collected for several other initial levels; in all cases, this propensity was observed.

This strong propensity to conserve the fine-structure/Λ-doublet label in rotationally inelastic collisions of CN($A^2\Pi$, $v = 3$) with N_2 differs strongly with our previous observations,[9] both in experiments and quantum scattering calculations, of CN($A^2\Pi$, $v = 3$)−Ar collisions. In this system, a strong probability to change both the fine-structure and Λ-doublet labels was found. Indeed, significant state-to-state rate constants for transitions into all four fine-structure/Λ-doublet manifolds were observed.

Using the propensity rules derived from a general consideration of the quantum scattering equations,[1,27,28] this strong propensity to conserve the fine-structure/Λ-doublet label can be related to properties of the CN($A^2\Pi$, $v = 3$)−N_2 PES. In the Hund's case (a) limit, which applies to the levels investigated in this study, rotationally inelastic transitions which conserve the fine-structure/Λ-doublet label are enabled by the anisotropic part of the sum (V_{sum}) of the average of the A' and A'' PES (V_{sum}), while fine-structure changing transitions involve the difference (V_{dif}) of these PES. Our observation of a strong conservation of the fine-structure and Λ-doublet labels suggests

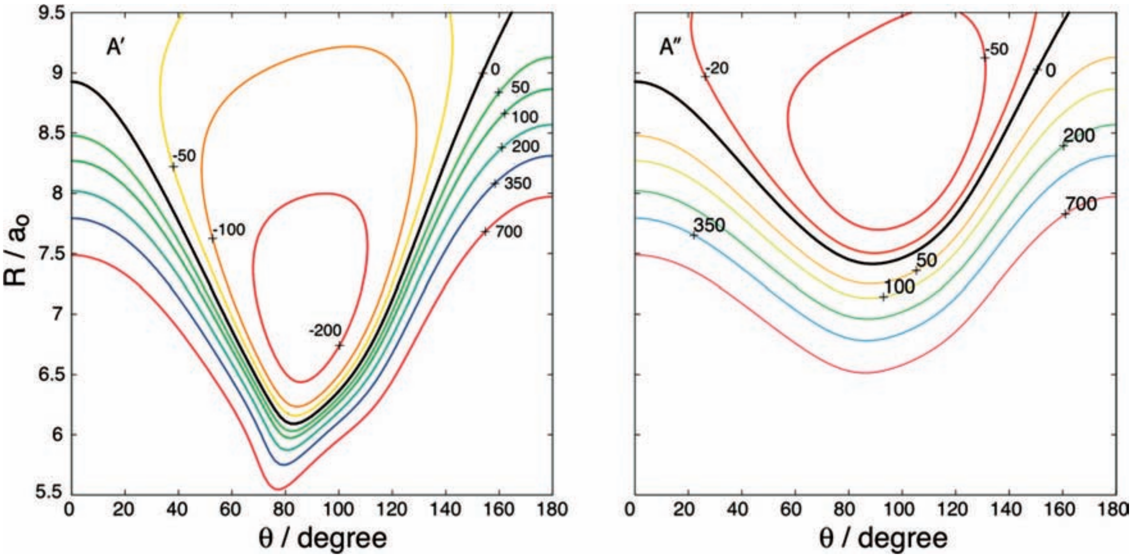

Figure 7. Contour plots (in cm^{-1}) of the CN(A)$-$N$_2$ PES as a function of the CN angle and the distance between the centers of mass of the two molecules, for the N$_2$ molecule fixed at linear geometry (geometry I), so that $\theta = 0$ corresponds to linear CNNN. The left and right panels correspond, respectively, to the states of A' and A'' reflection symmetry. The zero-energy heavy black contour separates the attractive and repulsive regions on the PES.

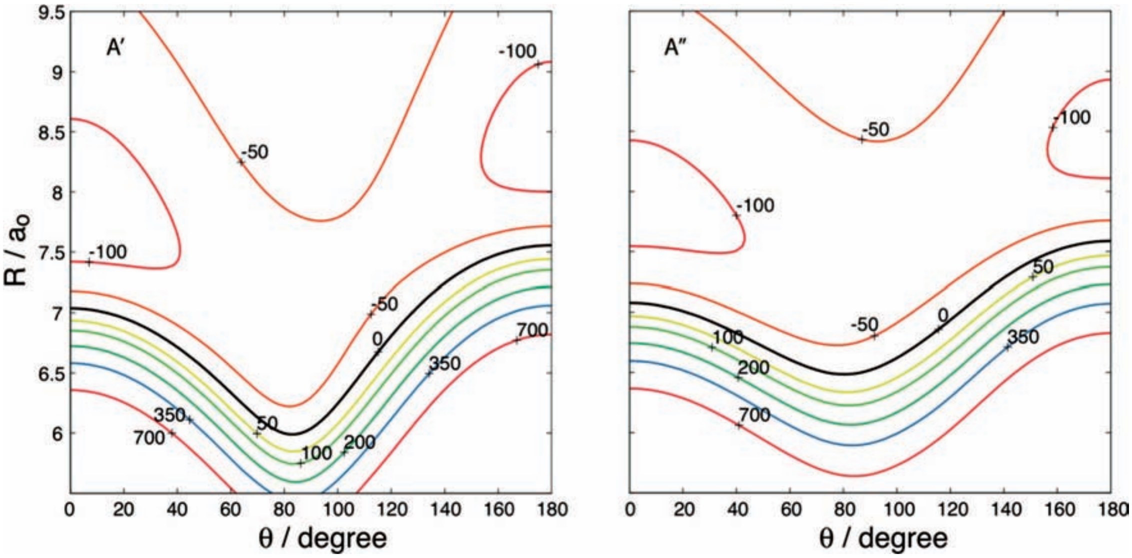

Figure 8. Contour plots (in cm^{-1}) of the CN(A)$-$N$_2$ PES as a function of the CN angle and the distance between the centers of mass of the two molecules, for the N$_2$ molecule fixed at perpendicular geometry but lying in the plane of the CN rotation (geometry II). Note that $\theta = 0$ corresponds to the N-end of the CN molecule pointing toward the N$_2$ molecule. The left and right panels correspond, respectively, to the states of A' and A'' reflection symmetry. The zero-energy heavy black contour separates the attractive and repulsive regions on the PES.

that V_{dif} is relatively small for this system. It will be interesting to see whether these suppositions hold true in the theoretical investigation of the interaction of CN($A^2\Pi$) with N$_2$ and computed state-to-state rate constants, presented in section 5.

4. Ab Initio Potential Energy Surfaces

Approach of a closed-shell target to a molecule in a $^2\Pi$ electronic state lifts the asymptotic degeneracy, so that two potential energy surfaces are needed to describe the collision.[27] For a spherical collision partner, the two states correspond to different reflection symmetries in the triatomic plane (A' and A''). These correspond to the odd π-electron located in or perpendicular to the triatomic plane, respectively. When the collision partner is a diatomic molecule, there are no symmetry elements for general geometries, so that an ab initio calculation would yield two states of A_1 symmetry. To describe completely the collision dynamics would require additional information to connect these two states with the two possible two-state orientations of the three CN π electrons.[29−31]

We shall adopt a simpler approach here, based on the analysis of the interaction of the SiS molecule with H$_2$.[32] We shall first assume that both the CN and N$_2$ molecules are frozen at their equilibrium internuclear distances, so that the PES is a function of only four coordinates: R, the distance between the centers of mass of the two diatomics; two polar angles θ and θ' which are the orientations with respect to $\boldsymbol{R}$ of the CN and NN bond, respectively; and ϕ, the dihedral angle. We shall further replace the molecule$-$molecule PES by the interaction of CN with a spherical target, by averaging the potential energy surface over all possible orientations of the N$_2$ molecule (over all possible values of θ' and ϕ). This spherical average is (crudely) obtained

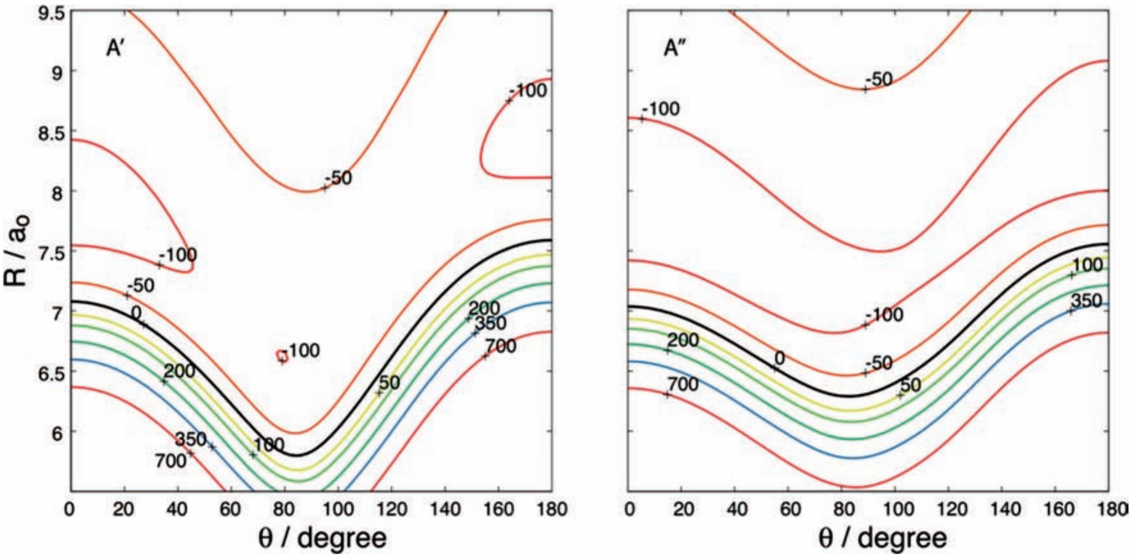

Figure 9. Contour plots (in cm^{-1}) of the CN(A)−N$_2$ PES as a function of the CN angle and the distance between the centers of mass of the two molecules, for the N$_2$ molecule fixed at perpendicular geometry and lying perpendicular to the plane of the CN rotation (geometry III). Note that the left and right panels correspond, respectively, to the states of A' and A'' reflection symmetry. The zero-energy heavy black contour separates the attractive and repulsive regions on the PES.

TABLE 2: Minima on the CN-N$_2$PES's

	geometry^a			
	I^b		II^c	
	A'	A''	A'	A''
R_m	6.98	8.31	7.87	7.89
θ_m	88	101	0	0
E_m	−282	−78	−125	−114

[a] See section 4, energy in cm^{-1}, distance in a_0, angle in degrees, with $\theta = 0$ corresponding to the N-end of the CN molecule pointing toward the N$_2$ molecule. [b] $\{\theta',\phi\} = \{0,0\}$. [c] $\{\theta',\phi\} = \{\pi/2,0\}$. One can show that for collinear CN, the minima for geometry III [$\{\pi/2, \pi/2\}$] are identical to those for geometry II, *except* that the reflection symmetry of the two states are reversed.

as the arithmetic average of the PES over three high-symmetry geometries, namely

$$\bar{V}_\Gamma(R,\theta) = \frac{1}{3}\sum_{n=1}^{3} V_\Gamma(R,\theta,\theta_n',\varphi_n) \qquad (2a)$$

where the three high symmetry geometries, which we shall designate I, II, and III, are defined by $\{\theta_n', \phi_n\} = \{0,0\}$, $\{\pi/2,0\}$, and $\{\pi/2, \pi/2\}$, where the subscript Γ designates the reflection symmetry. These geometries are illustrated in Figure 6. The first two geometries are coplanar, so that the two orientations of the π hole on the CN correspond to two different reflection symmetries. Similarly, a plane of reflection also exists for the third geometry, in which the N$_2$ molecule lies perpendicular to the plane in which the CN molecule is oriented.

Ab initio calculations were carried out for 40 values of R, ranging from 5 to 20 a_0, and for a 30° grid in the CN polar angle θ over the range of 0−180°. To determine the interaction energy, we used single-reference Hartree−Fock calculations followed by unrestricted coupled-cluster calculations with inclusion of single and double excitations and the perturbative inclusion of triple excitations [UCCSD(T)]. Upon approach of the N$_2$ collision partner, the symmetry of the $^2\Pi$ state of CN is lowered, so that the component of this state with A' reflection symmetry is no longer the lowest electronic state of its symmetry. However, the relatively weak interaction does not break significantly the orthogonality of the CN orbitals so that it is possible to converge the UCCSD(T) calculations of the CN(A)N$_2$ without variational collapse to the ground state. This is extremely advantageous, because a method which includes, even if just perturbatively, triple excitations will recover more of the dynamic correlation energy than a complete-active-space, self-consistent-field, multireference, configuration-interaction (CASSCF+MRCI) method, and is, in addition, size-consistent.

The UCCSD(T) calculations were done with an augmented, correlation-consistent, triple-ζ (avtz) atomic orbital basis.[33] To improve the description of the weak van der Waals interaction, we added a set of midbond functions[34] located at the midpoint of the Jacobi vector R. For this, we used three s and three p functions with exponents 0.9, 0.3, and 0.1 and two d functions with exponents 0.6 and 0.2.[35]

Following the description of the interaction between a molecule in a Π electronic state and a spherical target,[27] we use the average and half-difference of the spherically averaged PESs corresponding to the states of A' and A'' reflection symmetry, namely[27]

$$V_{\text{sum}}(R,\theta) = \frac{1}{2}[\bar{V}_{A''}(R,\theta) + \bar{V}_{A'}(R,\theta)] \qquad (3)$$

and

$$V_{\text{dif}}(R,\theta) = \frac{1}{2}[\bar{V}_{A''}(R,\theta) - \bar{V}_{A'}(R,\theta)] \qquad (4)$$

Figures 7−9 display contour plots of the CN−N$_2$ PES of for the states of A' and A'' reflection symmetry for the three high-symmetry geometries. We note that for collinear CN ($\theta = 0$ and π) the $\{\pi/2,0\}$ and $\{\pi/2, \pi/2\}$ geometries are degenerate. For all three geometries, there is substantial anisotropy in the repulsive wall which favors a bent CN orientation. As might be expected, this is more pronounced for geometry I, where the N$_2$ molecule is pointed directly toward the CN moiety. For all geometries, the anisotropy is greater for the state of A' reflection symmetry. For geometry I, the van der Waals minimum lies in bent geometry, but for geometries II and III, in linear geometry. In all three cases this corresponds to

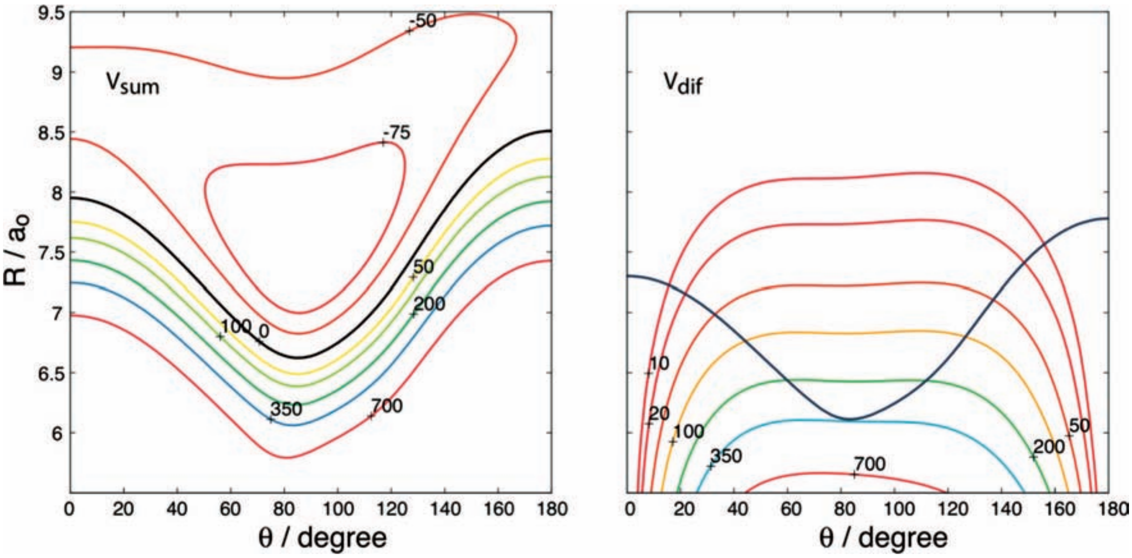

Figure 10. Contour plots (in cm^{-1}) of V_{sum} (eq 3) and V_{dif} (eq 4) of the averaged CN(A)$-N_2$ PES (eq 2) as a function of the CN angle and the distance between the centers of mass of the two molecules. Note that $\theta = 0$ corresponds to the N-end of the CN molecule pointing toward the N_2 molecule. On the left panel the zero-energy heavy black contour separates the attractive and repulsive regions on the PES. On the right panel, the heavy blue contour corresponds to 300 cm^{-1}, and so would delineate the classical turning point at a collision energy of 300 cm^{-1}.

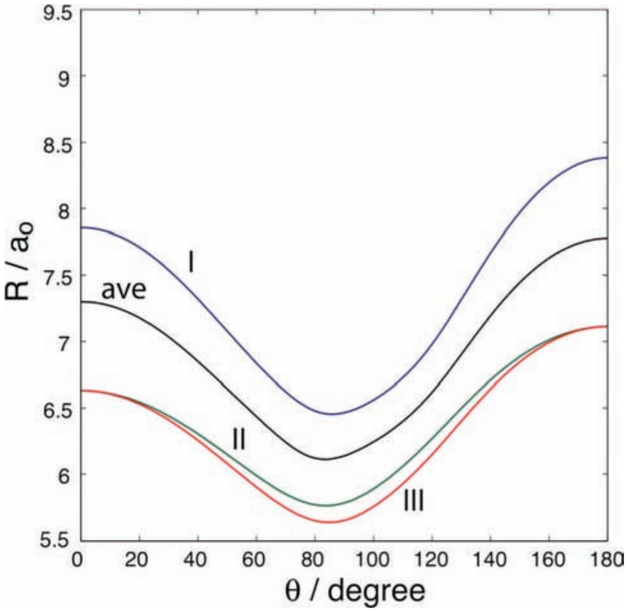

Figure 11. Locus of classical turning points for the average (V_{sum}) PES for each of the three geometries and for the averaged PES (black curve). Note that $\theta = 0$ corresponds to the N-end of the CN molecule pointing toward the N_2 molecule.

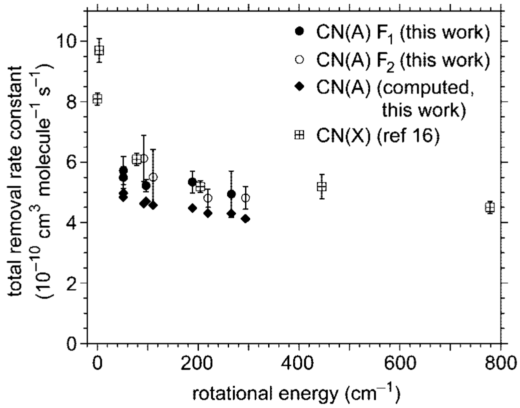

Figure 12. Total removal rate constants for specified levels in the CN($A^2\Pi$, $v = 3$) and CN($X^2\Sigma^+$, $v = 2$) manifolds plotted as a function of the rotational energy in the vibronic manifold: solid circles, CN(*A*), F_1 levels (this work); open circles, CN(*A*), F_2 levels (this work); diamonds, computed CN(*A*) rate constants (this work); squares, CN(*X*) (ref 16 with NCNO as the photolytic precursor).

T-shaped geometry. The positions of the minima on the CN(*A*)$-N_2$ PES for geometries I, II, and III are listed in Table 2.

Figure 10 displays comparable contour plots of the sum and difference PESs determined from the average of the PESs over the orientation of the N_2 molecule. By comparison with Figures 7−9, we see that the shape of the anisotropy in the averaged V_{sum} potential mirrors quite well the dependence on angle of the interaction potential. This is revealed more clearly by Figure 11, which shows the locus of turning points at a collision energy of 300 cm^{-1} for the average (V_{sum}) of the potentials for geometries I, II, and III, and for the V_{sum} of the averaged PES (eq 2).

We use the reproducing kernel Hilbert space (RKHS) method[36,37] to construct an analytic representation of the V_{sum} and V_{dif} PES needed for the scattering calculations. We construct the necessary two-dimensional kernel as a product of two one-dimensional kernels spanning, separately, the radial and angular coordinates, in a manner similar to that described in our recent work on the Na^+-H_2 complex.[38] At some values of the angle θ, it was not possible to converge the UCCSD(T) calculations for values of R less than $5a_0$, likely because of intruder electronic states at these short CN$-N_2$ distances. At these geometries it was necessary to add an exponential extrapolation of the PES for $R < 5a_0$ to ensure that the RKHS interpolated PES did not become unphysically attractive at small R.

5. Collision Dynamics

Collisions of CN(*A*) with spherically averaged N_2 are formally identical to collisions of a $^2\Pi$ molecule with a spherical atom, which we have studied extensively in the past.[27,39−41] We used the full close-coupling method to determine inelastic cross sections for the scattering of CN(*A*) by collision with spherical N_2, described by the sum and difference PESs defined eqs 3 and 4.[28,39] Cross sections were calculated by means of the

HIBRIDON 4.3 program suite.[42] Inelastic cross sections were determined over a large grid of collision energies.[41] Subsequent averaging over a Boltzmann distribution of collision energies yielded room temperature rate constants, as follows[43]

$$k_{JF_i\varepsilon\to J'F'_i\varepsilon'}(T)=\left(\frac{8}{\pi\mu k^3T^3}\right)^{1/2}\int_0^\infty \sigma_{JF_i\varepsilon\to J'F'_i\varepsilon'}(E)E\exp(-E/kT)\,\mathrm{d}E \quad (5)$$

where the CN rotational levels are labeled by the rotational quantum number J, the spin−orbit manifold label F_i, and the parity index ε. Here, k is Boltzmann's constant, μ is the collision reduced mass, and E is the collision energy. Total inelastic removal rates are obtained by summing over all energetically accessible final states, including the Λ-doublet changing, but J- and F_i-conserving, transitions.

Figures 4 and 5 display calculated rate constants for final-state-resolved transitions out of, respectively, the $J = 7.5$ F_1f and $J = 9.5$ $F_2\,f$ levels of CN(A, $v = 3$). The calculated total removal rate constants are listed in Table 1.

6. Discussion

The experimentally determined total removal rate constants reported in Table 1 are found to be much larger than the previously determined[21] rate constant for electronic quenching of CN($A^2\Pi$, $v = 3$) by N_2. From the ratio of these rate constants, we conclude that quenching comprises only ~4% of the loss of the initially prepared population in the specified rotational/fine-structure level. Hence, the initial level is depopulated predominantly by rotationally inelastic collisions, as expected.

It is of interest to compare the measured CN($A^2\Pi$, $v = 3$) total removal rate constants with those measured by Olkhov and Smith[16] for CN($X^2\Sigma^+$, $v = 2$). Figure 12 presents a plot of both sets of rate constants, plotted as a function of the rotational energy in each manifold. Also plotted in Figure 12 are our computed total removal rate constants. For both electronic states, the total removal rate constants show a decrease in magnitude as the rotational energy is increased. This behavior is commonly observed, as illustrated by CN(X, A)−Ar, He total removal rate constants,[8,9,13,14], and is a result of the increasing spacing between successive rotational energy levels with increasing J.

We also see in Figure 12 that the magnitudes of the total removal rate constants are remarkably similar for collisions of CN($A^2\Pi$, $v = 3$) and CN($X^2\Sigma^+$, $v = 2$) with N_2. Rotationally inelastic collisions within these two electronic states are enabled principally by the anisotropy of the repulsive parts of V_{sum} for the former and of the single PES for the latter. The similar magnitudes of the total removal rate constants suggest that the strengths of the anisotropies in the two systems are similar.

The total removal rate constants for CN($A^2\Pi$, $v = 3$)−N_2 collisions are somewhat larger than those previously measured for CN($A^2\Pi$, $v = 3$)−Ar.[9] For the one level which was investigated in both studies ($J = 7.5$ F_1f), the rate constant was measured experimentally to equal 3.42 ± 0.20 and computed theoretically as 3.75 (both in units of 10^{-10} cm^3 molecule^{-1} s^{-1}) for CN(A)−Ar collisions. It is more appropriate to compare thermally averaged cross sections (rate constant divided by average relative velocity). Taking into account the slight differences in CN−N_2 and CN−Ar reduced masses, the CN(A)−Ar cross section is ~30% smaller than that of CN(A)−N_2. The differences in the CN(X)−Ar and CN(X)−N_2 total removal cross section are much less than this. Nevertheless, the dependence of the computed rate constants upon rotational level mirrors that of the measured rate constants.

Comparison of the experimental and computed rate constants shows that the calculated removal rate constants are close in magnitude to the experimental value but 10−15% smaller. Part of this difference can be attributed to the neglect of the electronic quenching channel in the theoretical simulations. Also, we have used a PES which has been averaged over the orientation of the N_2 partner. This will certainly reduce the overall anisotropy of the interaction. Third, we have the neglected the rotational inelasticity of the N_2 partner, which will certainly contribute to the overall removal rate.

Turning our attention to the rate constants for state-to-state rotational energy transfer, we observe in Figures 4 and 5 that the experimental CN($A^2\Pi$, $v = 3$)−N_2 data show a strong propensity to conserve both the initial fine-structure manifold and the initial Λ-doublet labels. This behavior is in sharp contrast to the rate constants for CN($A^2\Pi$, $v = 3$)−Ar state-to-state transitions, which show similar magnitudes for transitions involving conservation and change of the fine-structure and Λ-doublet labels.[9] We see in Figures 4 and 5 that the theoretical calculations predict a similar dependence on the final rotational quantum number for transitions which conserve the initial fine-structure and Λ-doublet label. However, for transitions which change either (or both) of these labels, the theoretical calculations predict much larger rate constants and thus do not confirm the remarkable propensity seen experimentally.

In the Hund's case (a) limit, fine-structure changing transitions are induced by the difference between the PES corresponding to states of A' and A'' symmetry.[39] As can be seen in Figures 7−9 for the CN($A^2\Pi$, v = 3)−N_2 system, these PESs are quite different, and one would hence anticipate sizable rate constants for fine-structure changing transitions. It is also curious that the calculations show that the efficiency of inelastic energy transfer within both the F_1 (Figure 4) and F_2 (Figure 5) fine-structure manifolds is roughly independent of the Λ-doublet label for the final state, in contrast to experiment. As mentioned above, the theoretical simulations are based on a PES which has been averaged over the orientation of the N_2 partner and, in addition, neglect all rotational inelasticity of the N_2 partner. It may well be that these simplifications are responsible for the disagreement with experiment.

In the astrophysics community, there is considerable interest in the use of rate constants for atom−molecule rotational energy transfer to model energy transfer in molecule−molecule encounters.[32] The comparison with theory presented here, and the comparison with our earlier work on collisions of CN($A^2\Pi$, v = 3) with Ar, reveal clear difficulties in the use of atom-based simulations for the study of resonance energy transfer in collisions with molecular targets.

References and Notes

(1) Dagdigian, P. J. In *The Chemical Dynamics and Kinetics of Small Radicals, Part I*; Liu, K., Wagner, A. F., Eds.; World Scientific: Singapore, 1995; p 315.

(2) Furio, N.; Ali, A.; Dagdigian, P. J. *Chem. Phys. Lett.* **1986**, *125*, 561.

(3) Furio, N.; Ali, A.; Dagdigian, P. J. *J. Chem. Phys.* **1986**, *85*, 3860.

(4) Jihua, G.; Ali, A.; Dagdigian, P. J. *J. Chem. Phys.* **1986**, *85*, 7098.

(5) Ali, A.; Jihua, G.; Dagdigian, P. J. *J. Chem. Phys.* **1987**, *87*, 2045.

(6) Dagdigian, P. J.; Patel-Misra, D.; Berning, A.; Werner, H.-J.; Alexander, M. H. *J. Chem. Phys.* **1993**, *98*, 8580.

(7) Yang, X.; Dagdigian, P. J. *Chem. Phys. Lett.* **1998**, *297*, 506.

(8) Yang, X.; Dagdigian, P. J.; Alexander, M. H. *J. Chem. Phys.* **2000**, *112*, 4474.

(9) Alexander, M. H.; Yang, X.; Dagdigian, P. J.; Berning, A.; Werner, H.-J. *J. Chem. Phys.* **2000**, *112*, 781.

(10) Nizamov, B.; Dagdigian, P. J.; Alexander, M. H. *J. Chem. Phys.* **2001**, *115*, 8393.

(11) Alagappan, A.; Ballingall, I.; Costen, M. L.; McKendrick, K. G.; Paterson, G. *Phys. Chem. Chem. Phys.* **2007**, *9*, 747.

(12) Alagappan, A.; Ballingall, I.; Costen, M. L.; McKendrick, K. G. *J. Chem. Phys.* **2007**, *126*, 041103.

(13) Fei, R.; Lambert, H. M.; Carrington, T.; Filseth, S. V.; Sadowski, C. M. *J. Chem. Phys.* **1994**, *100*, 1190.

(14) Fei, R.; Adelman, D. E.; Carrington, T.; Dugan, C. H.; Filseth, S. V. *Chem. Phys. Lett.* **1995**, *232*, 547.

(15) Hickson, K. M.; Sadowski, C. M.; Smith, I. W. M. *Chem. Phys. Lett.* **2003**, *372*, 443.

(16) Olkhov, R. V.; Smith, I. W. M. *Phys. Chem. Chem. Phys.* **2006**, *8*, 5643.

(17) Guo, J. Z.; Sadowski, C. M.; Gao, Q.; Morgan, F. J. *J. Chem. Phys.* **2000**, *113*, 7276.

(18) Brunet, S. M. K.; Guo, J. Z.; Carrington, T.; Filseth, S. V.; Sadowski, C. M. *J. Chem. Phys.* **2002**, *116*, 3617.

(19) Conley, C.; Halpern, J. B.; Wood, J.; Vaughn, C.; Jackson, W. M. *Chem. Phys. Lett.* **1980**, *73*, 224.

(20) Taherian, M. R.; Slanger, T. G. *J. Chem. Phys.* **1985**, *82*, 2511.

(21) Halpern, J. B.; Huang, Y.; Titarchuk, T. *Astrophys. Space Sci.* **1996**, *236*, 11.

(22) Guyer, D. R.; Hüwel, L.; Leone, S. R. *J. Chem. Phys.* **1983**, *83*, 1259.

(23) Hossenlopp, J. M.; Anderson, D. T.; Todd, M. W.; Lester, M. I. *J. Chem. Phys.* **1998**, *109*, 10707.

(24) Olkhov, R.; Smith, I. W. M. *J. Chem. Phys.* **2007**, *126*, 134314.

(25) Kotlar, A. J.; Field, R. W.; Steinfeld, J. I.; Coxon, J. A. *J. Mol. Spectrosc.* **1980**, *80*, 86.

(26) Brown, J. M.; Hougen, J. T.; Huber, K.-P.; Johns, J. W. C.; Kopp, I.; Lefebvre-Brion, H.; Merer, A. J.; Ramsay, D. A.; Rostas, J.; Zare, R. N. *J. Mol. Spectrosc.* **1975**, *55*, 500.

(27) Alexander, M. H. *Chem. Phys.* **1985**, *92*, 337.

(28) Corey, G. C.; Alexander, M. H. *J. Chem. Phys.* **1986**, *85*, 5652.

(29) Corey, G. C.; Alexander, M. H. *J. Chem. Phys.* **1988**, *88*, 6931.

(30) Corey, G. C.; Alexander, M. H.; Dagdigian, P. J. *J. Chem. Phys.* **1986**, *84*, 1547.

(31) Wormer, P. E. S.; Klos, J. A.; Groenenboom, G. C.; van der Avoird, A. *J. Chem. Phys.* **2005**, *122*, 244325.

(32) Lique, F.; Tobola, R.; Klos, J.; Feautrier, N.; Spielfiedel, A.; Vincent, L. F. M.; Chalasinski, G.; Alexander, M. H. *Astron. Astrophys.* **2008**, *478*, 567.

(33) Dunning, T. H., Jr. *J. Chem. Phys.* **1989**, *90*, 1007.

(34) Tao, F.-M.; Pan, Y.-K. *J. Chem. Phys.* **1992**, *97*, 4989.

(35) Burcl, R.; Chalasinski, G.; Bukowski, R.; Szczesniak, M. M. *J. Chem. Phys.* **1995**, *103*, 1498.

(36) Ho, T. S.; Rabitz, H. *J. Chem. Phys.* **1996**, *104*, 2584.

(37) Hollebeek, T.; Ho, T.-S.; Rabitz, H. *Annu. Rev. Phys. Chem.* **1999**, *50*, 537.

(38) Poad, B. L. J.; Wearne, P. J.; Bieske, E. J.; Buchachenko, A. A.; Bennett, D. I. G.; Klos, J.; Alexander, M. H. *J. Chem. Phys.* **2008**, *129*, 184306.

(39) Alexander, M. H. *J. Chem. Phys.* **1982**, *76*, 5974.

(40) Alexander, M. H. *J. Chem. Phys.* **1993**, *99*, 7725.

(41) Islam, M.; Smith, I. W. M.; Alexander, M. H. *Phys. Chem. Chem. Phys.* **2000**, *2*, 473.

(42) HIBRIDON is a package of programs for the time-independent quantum treatment of inelastic collisions and photodissociation written by M. H. Alexander, D. E. Manolopoulos, H.-J. Werner, and B. Follmeg with contributions by P. F. Vohralik, D. Lemoine, G. Corey, B. Johnson, T. Orlikowski, W. Kearney, A. Berning, A. Degli-Esposti, C. Rist, and P. Dagdigian. More information and/or a copy of the code can be obtained from the website http://www.chem.umd.edu/groups/alexander/hibridon/hib43.

(43) Smith, I. W. M. *Kinetics and Dynamics of Elementary Gas Reactions*; Butterworths: London, 1980.

JP810148W